A recursive filter for 3D MAP reconstruction

João Sanches *Jorge S. Marques*

Instituto Superior Técnico / Instituto de Sistemas e Robótica
Av. Rovisco Pais, 1049-001
Lisboa, Portugal

***Abstract* – Three dimensional reconstruction aims at estimating a real function f defined on a subset of R^3. The function f usually conveys information about the organs properties to be used for medical diagnosis. Bayesian methods (e.g. MAP) are often used to address this problem since they allow to incorporate the available knowledge about the data and function to be estimated. However they are usually slow and exhibit a bad performance at transitions. This paper addresses both difficulties by approximating the MAP solution by the output of a set of recursive filters which are fast and provide better results at transitions.**

***Keywords* – 3D Reconstruction, MAP, IIR Filter, Medical Imaging**

I. Introduction

3D reconstruction aims at estimating a 3D function $f : \Omega \rightarrow R$ where $\Omega \subset R^3$ is a 3D region of interest (e.g., a region of the human body). This problem arises in several biomedical applications e.g., CT, MRI and Ultrasound imaging.

The function to be reconstructed f is usually observed at a discrete set of points $x_i \in R^3$ and only noisy observations y_i are usually available. The problem can then be formulated as follows: given a set of data $V = \{x_i, y_i\}$ we wish to estimate f in the region of interest Ω.

Several methods have been proposed to address this problem [1]-[6].

The Bayesian methods are one of the most popular solution since they provide a sound framework to incorporate the available information about the data model and about the a priori knowledge on f. They have however some disadvantages: they are usually slow and exhibits a bad performance at transitions if Gaussian priors [7] are used [8]-[13].

This paper addresses both difficulties by approximating the MAP solution by the output of a set of recursive filters which are fast and allow a better representation of the transitions.

II. MAP Reconstruction

Let $f(x)$ be a function to be estimated, defined in $\Omega \subset R^3$. It is assumed that f interpolates a set of coefficients $u_1, u_2, ..., u_N$ defined on the nodes of a cubic grid. Therefore, f can be expressed as follow

$$f(x) = \Phi(x)^T U \tag{1}$$

where $\Phi(x) = [\phi_1(x), \phi_2(x), ..., \phi_N(x)]^T$ is a vector of interpolating functions and $U = [u_1, u_2, ..., u_N]$ is a $N \times 1$ vector of coefficients. The coefficients u_p form a discrete 3D signal defined in $R^3 \cap \Omega$.

Let $V = \{x_i, y_i\}$ be the set of observed data: y_i being a noisy observation of $f(x_i)$ and $x_i \in \Omega$. Let us assume that the observations y_i are independent random variables with normal distribution,i.e.,

$$p(y_i/x_i) = \frac{1}{\sqrt{2\pi\sigma^2(x)}} \frac{(y_i - f(x_i))^2}{2\sigma^2(x)} \tag{2}$$

where it is assumed that x_i is accurately measured and that the mean $f(x)$ and variance $\sigma^2(x)$ change in Ω. The likelihood function is

$$l(V, U) = C - \sum_i \left(\frac{(y_i - f(x_i))^2}{2\sigma^2(x_i)} + \log \sigma^2(x_i)\right) \tag{3}$$

where $C = -\frac{N}{2} \log 2\pi$ and $\sigma^2(x_i)$ is assumed to be constant in the vicinity of u_p and computed from the data points that intersect that vicinity (voxel).

In this paper U is modeled as a Markov random field with a Gibbs distribution ,

$$p(U) = \frac{1}{Z} e^{-\frac{\alpha}{N'_v} \sum_{p \in G} \sum_{g \in \delta'_p} (u_p - u_g)^2} \tag{4}$$

where Z is the partition function, G is the set of indexes of the U coefficients and δ'_p is the set of all N'_v backwards neighbors of u_p. This prior constraints neighboring values penalizing differences between neighboring nodes. By selecting the regularization parameter α it is possible to control the degree of smoothness of the solution and therefore its bandwidth [14].

3D reconstruction aims to estimate U using the observations $v_i = (y_i, x_i)$. In the popular method MAP algorithm the solution is obtained as follows

$$\hat{U} = arg \max_U E(U, V) \tag{5}$$

where

$$E(U, V) = -l(U, V) - \log\left(p(U)\right) \tag{6}$$

This work was partially supported by FCT in the scope of the project Heart 3D. Corresponding author: João Sanches, E-mail: jmrs@alfa.ist.utl.pt

The solution of (5) corresponds to an huge optimization problem that usually is solved by using numerical methods. Since U has thousands of coefficients the optimization procedure is computationally demanding. The ICM [15] algorithm has been used to address this problem. This algorithm transforms the N-dimensional optimization problem in a set collection of 1-D optimization problems (see [14] for details).

The optimization of (5) with respect to each volume coefficient u_p is performed by finding the stationary point of E with respect to u_p, i.e.,

$$\frac{\partial E(V,U)}{\partial u_p} = 0 \tag{7}$$

Using the fixed point method an iterative algorithm can be found

$$u_p = \frac{1}{4\alpha}\sum_i \frac{f(x_i)-y_i}{\sigma^2(x_i)}\phi_p(x_i) + \bar{u}_p \tag{8}$$

The MAP estimation using (8) is usually slow and has a limited convergence range. To enforce the convergence the initial volume and the regularization parameter must be carefully chosen.

To overcome these difficulties a simplification to this algorithm is proposed in the next section by deriving an IIR filter. The estimation process using this recursive filter becomes a non iterative process, more stable and faster than the previous method.

III. IIR MAP FILTER

In this section a set of IIR filters are derived which approximate the MAP estimate.

Let us consider (8). If $f(x)$ is smooth it can be approximated by u_p in the vicinity of the p-th node, i.e.,

$$f(x_i) \simeq u_p \tag{9}$$

leading to

$$u_p = \frac{1}{4\alpha}[u_p \sum_i \frac{\phi_p(x_i)}{\sigma^2(x_i)} - \sum_i \frac{y_i\phi_p(x_i)}{\sigma^2(x_i)}] + \bar{u}_p \tag{10}$$

This can be rewritten as

$$u_p = (1-k_p)u_p^{ML} + k_p\bar{u}_p \tag{11}$$

where

$$k_p = \frac{1}{1+\sum_i \frac{\phi_p(x_i)}{4\alpha\sigma^2(x_i)}} \tag{12}$$

$$u_p^{ML} = \frac{\sum_i y_i\phi_p(x_i)}{\sum_i \phi_p(x_i)} \tag{13}$$

The equation (11) defines an IIR filter. However, since it is not wedge supported [16], i.e., the output depends on past and futures outputs, it is not possible to compute it recursively. To overcome this difficulty (11) will be replaced by a set of eight wedge supported filters which can be recursively computed,

$$u_p^w = (1-k_p)u_p^{ML} + k_p u^{\bar{w}}{}_p \tag{14}$$

where $w = 1,..,8$, $p = (i,j,k)$ and $u^{\bar{w}}{}_p$ is the mean of the three backward neighbors of u_p with respect to the direction of sweeping. Each filter is recursively computed starting from a different corner of the tri-dimensional grid as shown in Fig.1. The outputs of these filters are then averaged to produce the final result as shown in Fig.2. This approach does not provide the true MAP solution but, as we will show in the section of experimental results, it still achieves very good results. Furthermore, it has the advantage of being always stable.

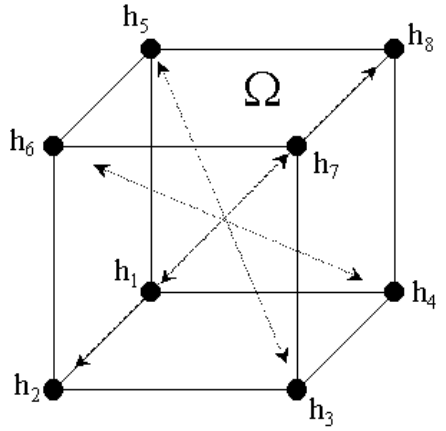

Figure 1 - Starting points of the IIR filters.

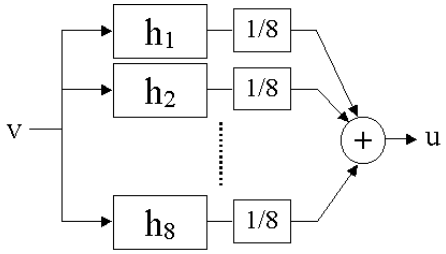

Figure 2 - Bank of recursive filters used to approximate the non wedge MAP filter.

IV. FREQUENCY RESPONSE

Let us consider one of the wedge supported filters, e.g., h_1 and let us consider the 1D equivalent filter, i.e.,

$$u_n = (1-k_n)u_n^{ML} + k_n u_{n-1} \tag{15}$$

.

Assuming that k_n is constant and equal to k in a small vicinity of the nth node the z-transform of h_1 is

$$H_1(Z) = \frac{1-k}{1-kZ^{-1}} \tag{16}$$

This is the expression of a first order low-pass filter with unit gain at $\omega = 0$ and a pole at k (see Fig.4a)). This approach explains why the Gibbs prior with quadratic potential functions does not represents the transitions well. In fact, under this approach, the regularization imposed by the prior is equivalent to filtering the ML estimates with a first order low-pass filter smoothes the transitions (see Fig.3).

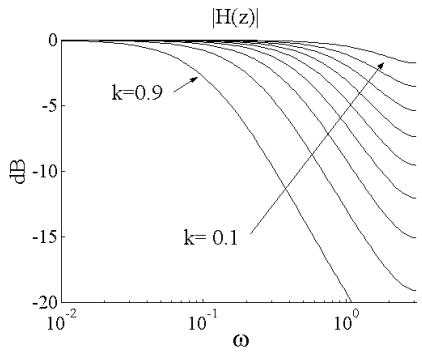

Figure 3 - Frequency response of the first order filter for different values of $k = 0.1, 0.2, ..., 0.9$

Some additional conclusions can be stated using (12): conclude that:

1) taking into account that $\phi_p(x_i) \geq 0$ then $0 \leq k_p \leq 1$ which means that the pole of the first order filter is always inside the unit circle, or , the filter is always stable.

2) the parameter k_p decreases with the number of data points with $\sum \phi_p(x_i)$, i.e., the bandwidth of the filter increases with the amount of available data and decreases as the number of data points goes to zero. The algorithm compensates the lack of confidence in the data by decreasing the filter bandwidth.

3) the bandwidth of the filter decreases with the increasing of the regulatization parameter α and with the increasing of the variance of the data in the vicinity of u_p, $\sigma^2(x)$.

4) the algorithm is implemented in such way that when there is no data $k_p = 1$. In this case $u_p = \bar{u}_p$, i.e., the node estimates is equal to the mean of the neighbors.

Therefore, the IIR filter proposed in this paper, is a space variant filter that adapts its bandwidth along space according to the amount of observed data and its uncertainty.

The first order filter is not appropriated to deal with transitions. In the next section, a new class of filter are proposed to improve the performance of the algorithm at the transitions.

V. Second Order Low Pass Filter

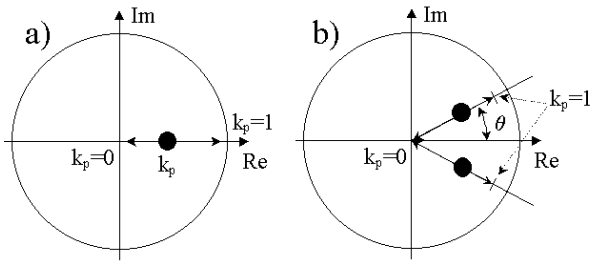

Figure 4 - Root locus. a)1st order IIR filter, b)2nd order IIR filter

The first order filters derived in the previous section have unit gain at $w = 0$ and a pole at k_p with $0 < k_p < 1$. Let now consider a second order IIR filter with complex poles at positions $k'_p = \lambda k_p e^{\pm j\theta}$, as shown in Fig.4.b) and with unit gain at $w = 0$. The parameter λ is used to avoid poles in the unit circumference which leads to instability ($\lambda = 0.9$).

This second order IIR filter should be design to have a larger bandwidth than the first order filter but a smaller transition region. In this case the transitions are better preserved and the high frequency noise better attenuated.

Fig.5 shows the frequency response for three different values of k_p. It is visible that the bandwidth of the second order IIR filter is smaller than the first order filter for small values of k_p (e.g. $k_p = 0.1$) and bigger for large values.

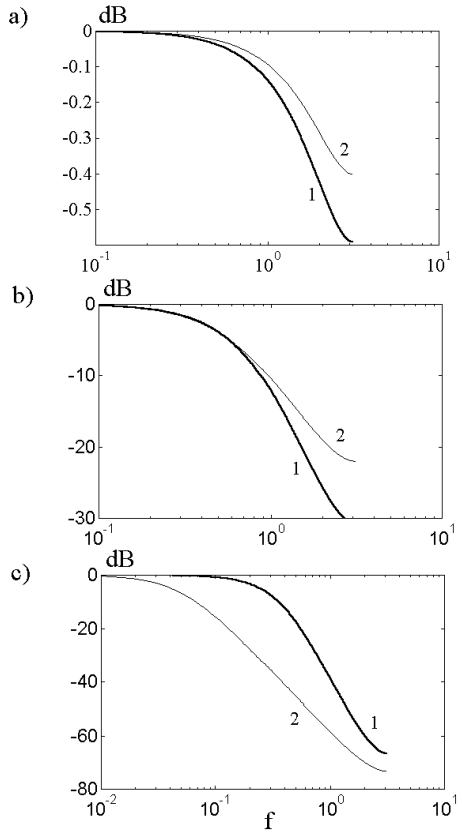

Figure 5 - Frequency response of first order(1) and second order(2) IIR filter for three different values of k_p; a)$k_p = 0.1$, b)$k_p = 0.5$ and c)$k_p = 0.95$ with $\lambda = 0.9$ and $\theta = 10$

The Z-transform of this second order filter is

$$H(Z) = \frac{1 - 2\lambda K_p cos(\theta) + (\lambda k_p)^2}{1 - 2\lambda K_p cos(\theta) Z^{-1} + (\lambda k_p)^2 Z^{-2}} \tag{17}$$

allows to derive the new recursive filter expression

$$u_p^w = g_p u_p^{ML} + \frac{1}{3} G_p^w \tag{18}$$

where $g_p = (1 - 2\lambda k_p cos(\theta) + (\lambda k_p)^2)$ and $G_p(u_p)$ is obtained by applying a mask involving the six backward neighbors of the p-th node as shown in Fig.6 where $a = 2\lambda k_p cos(\theta)$ and $b = -(\lambda k_p)^2$.

VI. Experimental Results

This section illustrates the performance of the proposed algorithm using synthetic and real data. In each experiment

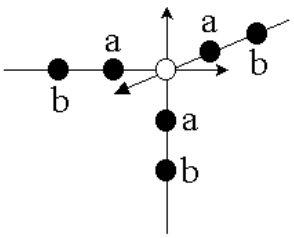

Figure 6 - Mask used in the second order filter. $a = 2\lambda k_p cos(\theta)$ and $b = -(\lambda k_p)^2$

Algorithm	L	S/N(dB)	Time(s)
MAP	-1.036e7	24.14	384.76
IIR 1st Ord	-1.028e7	24.20	19.60
IIR 2nd Ord	-1.027e7	27.69	19.58

Table I
SIMULATION RESULTS WITH SYNTHETIC DATA.

reconstructions are performed using the MAP method (8), the first order IIR filter (11) and the second order IIR filter (18). The reconstructions are shown as well as a set of figures of merit used to evaluate the algorithms: the likelihood, the processing time and the signal to noise ratio (in the case of synthetic data only) .

In the first experiment, a sequence of synthetic data is used consisting of 128 images with 128×128 pixel. These images correspond to parallel cross sections of a binary volume containing a sphere corrupted with white noise $w \sim N(0, 32^2)$. The background mean is 75 and the sphere mean is 150. Fig.7 shows the reconstruction results obtained with the three methods and the Table I shows the figures of merit used to evaluate them. Since it is difficult to visualize a 3D volume only 2D cuts and 1D profiles are shown. It is concluded that the 1st order filter achieves results similar to the MAP method being 20 times faster. This example shows that non iterative methods can be used to achieve good reconstruction results. The second order filter is as fast as the first order reconstruction and improves the reconstruction results at the transitions being therefore the best solution for this problem.

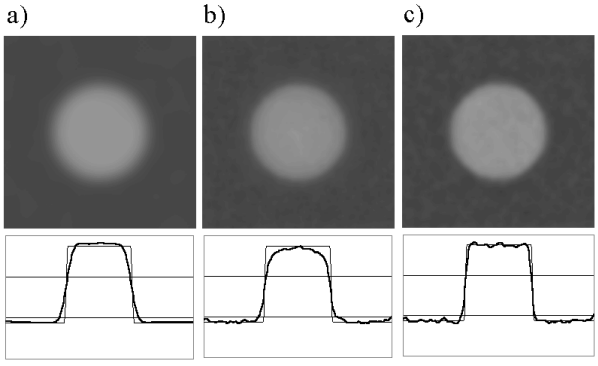

Figure 7 - Reconstruction results (2D cut and 1D profile) obtained with:a)MAP method, b)1st order filter and c) 2nd order filter.

Experimental tests were also performed using a set of 40 images[1] with 120×100 pixels of a cell nuclei obtained with the HRCM (high resolution cytometry) technique using an optical microscope [17]. The distance between slices is 0.2 micrometers and each pixel is of size 0.1 x 0.1 micrometer. The results are displayed in Fig.8 and Fig.9 and in table II.

Algorithm	L	Time(s)
MAP	-2.076e6	96.32
IIR 1st Ord	-2.044e6	5.60
IIR 2nd Ord	-2.044e6	5.60

Table II
SIMULATION RESULTS WITH REAL DATA.

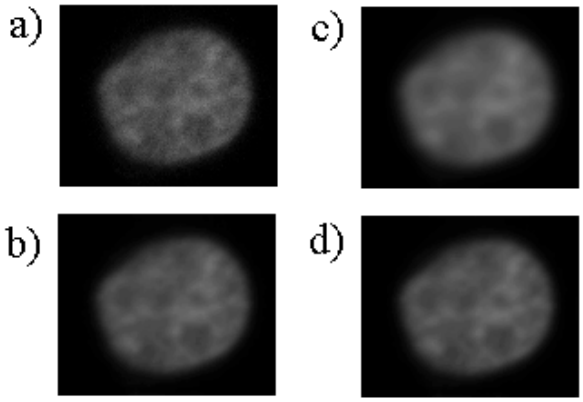

Figure 8 - Reconstruction results using real data. a)image belonging to the data sequence. Cross section extracted from the volume estimated using the b)MAP iterative method, c)1st order IIR filter and d)2nd order IIR filter.

Again the 1st order filter achieves similar results to the ones obtained with the MAP iterative method with significant(one order of magnitude) computational gains. The performance of the 2nd order filter is similar to the one obtained with the 1st order filter because, in this case of real data, there are no abrupt transitions.

Fig.10 shows the segmentation results. This results are obtained using ray-casting techniques applied to the volumes estimated using the MAP algorithm (see Fig.10a)) and the 2nd order IIR filter (see Fig.10b)). The 2nd order IIR filter presents artifacts that do not correspond to any anatomical detail. These artifacts, appearing as a structure of parallel contours, are due to an non perfect interpolation operation between the data planes. To value of the α parameter used in both methods, MAP and 2nd order IIR filter, is the same to allow a comparison. However, by increasing this value in the IIR filter method it is possible to reduce or even eliminate these artifacts.

VII. CONCLUSIONS

This paper presents a fast algorithm for 3D MAP reconstruction based on the use of recursive IIR filters. The algorithm performs as follows. First the maximum likelihood

[1]This sequence was gently provided by Pavel Matula from the Laboratory of Optical Microscopy, Faculty of Informatics, Masaryk University, Czech Republic

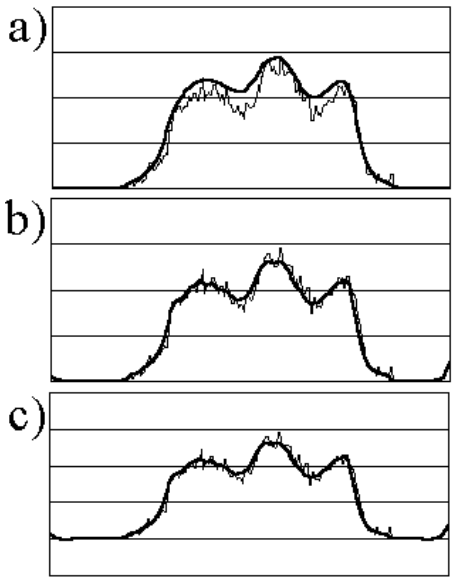

Figure 9 - 1D diagonal profiles. Comparison of the original image with the estimated images using a)MAP iterative method, b)1st IIR filter and c)2nd IIR filter.

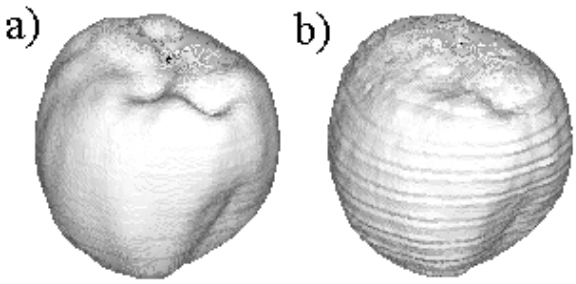

Figure 10 - Cell surfaces obtained with a)MAP method and b)2nd order IIR filter.

estimate of the volume coefficients is computed for every observed node of the 3D grid. Second, a set of 8 filters is applied to the ML estimates each of them starting from a different corner of the volume to be reconstructed. The proposed filters are space variant: they have a small bandwidth when a large number of observations are performed in the vicinity of a grid node and they have a large bandwidth in the case of few or zero observations. It has been shown that the proposed algorithm is much faster than the original MAP method, has better performance at the transitions and is more stable.

The methods described in this paper for a Gaussian data model can be easily applied with other types of distributions. An example is the Rayleigh distribution used in 3D ultrasound which leads to non linear optimization problems and can easily be tackled using the proposed technique [18].

REFERENCES

[1] T. Nelson, D. Downey, D. Pretorius, A. Fenster, Three-Dimensional Ultrasound, Lippincott, 1999.

[2] S.P. Raya, J.K. Udupa, Shape-Based Interpolation of Multidimensional Objects, IEEE Trans. on Medical Imaging, vol.9, no.1, pp3-42, March 1990.

[3] G.M.Treece, R.W.Preager, A.H.Gee and L. Berman, Fast surface and volume estimation from non-parallel cross-sections, for frehand 3-D ultrasound, Medical Image Analysis, vol.3, no.2, pp.141-173, 1999.

[4] T. McInerney and D. Terzopoulos, Deformable Models in Medical Image Analysis: a Survey, Medical Image Analysis, vol.1, Issue 2, pp.91-108, 1996.

[5] R.N.Rohling, A. H. Gee and L. Berman, A comparation of freehand three-dimensional ultrasound reconstruction techniques, Medical Image Analysis, vol.4, no.4, pp.339-359, 1999.

[6] T.R.Nelson, D.H.Pretorius, Interactive Acquisition, Analysis and Visualization of Sonographic Volume Data, International Journal of Imaging Systems and Technology, vol.8, pp.26-37, 1997.

[7] S. Geman et al., Stochastic Relaxation, Gibbs Distributions, and the Bayesian Restoration of Images, IEEE Trans on PAMI, vol.PAMI-6, no.6, pp.721-741, Nov. 1984.

[8] S. Geman and D. McClure, Bayesian Image Analysis: An Application to single photon emission tomography, Proc. Statist. Comput. Sect., Amer. Statist. Assoc. Washington, DC, pp.12-18, 1985.

[9] Peter J. Green, Bayesian Reconstructions From Emission Tomography Data Using a Modified EM Algorithm,IEEE Trans. on Medical Imaging, vol.9, no.1, March 1990.

[10] T. Herbert and R. Leahy, A Generalized EM Algorithm for 3D Bayesian Reconstruction from Poisson Data Using Gibbs Priors, IEEE Trans. on Medical Imaging, vol.8, no.2, June 1989.

[11] D.S.Lalush and B.M.W.Tsui, Simulation Evaluation of Gibbs Prior Distribution for Use in Maximum A Posteriori SPECT Reconstructions,IEEE Trans. on Medical Imaging, vol.11, no.2, June 1992.

[12] V.E.Johnson, W.H.Wong, X. Hu and C.T Chen, Image Restoration Using Gibbs Priors: Boundary Modeling, Tratment of Blurring, and Selection of Hyperparameter, Trans. PAMI, vol.13, no5, May 1991.

[13] S.Z.Li, Close-Form Solution and Parameter Selection for Convex Minimization-Based Edge-Preserving Smoothing, IEEE Trans. on PAMI, vol. PAMI-20, no.9, pp.916-932, September 1998.

[14] J. Sanches and J. S. Marques, A Rayleigh Reconstruction/Interpolation Algorithm for 3D Ultrasound, Pattern Recognition Letters, Elsevier, 21, pp.917-926, October, 2000.

[15] J. Besag, On the Statistical Analysis of Dirty Pictures, J. R. Statist. Soc. B, vol.48, no. 3, pp. 259-302, 1986.

[16] Jae. S. Lim, Two-Dimensional Signal and Image Processing, PTR Prentice Hall, Englewood Cliffs, New Jersey.

[17] P. Matula and D. Svoboda, Spherical Object Reconstruction Using Star-Shaped Simplex Meshes, Proceedings 3th EMMCVPR2001, pp.63-74, France, September 2001.

[18] J.Sanches and J.S. Marques, A Fast MAP Algorithm for 3D Ultrasound, Proceedings 3th EMMCVPR2001, pp.63-74, France, September 2001.